Geophysical Journal International

Geophys. J. Int. (2012) **190,** 829–842 doi: 10.1111/j.1365-246X.2012.05537.x

A precursor to the Matuyama–Brunhes reversal in Chinese loess and its palaeomagnetic and stratigraphic significance

Chunsheng Jin,[1] Qingsong Liu[1] and Juan Cruz Larrasoaña[2]

[1]*State Key Laboratory of Lithospheric Evolution, Institute of Geology and Geophysics, Chinese Academy of Sciences, Beijing* 100029*, China. E-mail: qsliu@mail.iggcas.ac.cn*

[2]*Instituto Geológico y Minero de España, Unidad de Zaragoza, C/Manuel Lasala* 44, 9B, *Saragossa* 50006*, Spain*

Accepted 2012 May 3. Received 2012 May 3; in original form 2011 October 11

SUMMARY

We report high-resolution palaeomagnetic results across the lower part of S8 in the Luochuan area, northwest of China using parallel subsets samples. A palaeomagnetic anomaly with low palaeointensity and disordered magnetic direction was identified ∼21 ka prior to the Matuyama–Brunhes (MB) polarity reversal, and is consistent with the MB precursor observed from marine sediments and lava flows. This is the first convincing report of the MB precursor in terrestrial material (Chinese loess), which attests the global feature of the MB precursor. Constrained by the stratigraphic position of both the MB polarity reversal and the MB precursor, the loess unit L8 and palaeosol unit S8 of the Chinese loess sequence are undoubtedly tied to the marine isotope stages 18 and 19, respectively. This correlation is critical for an accurate understanding of the correspondences of palaeomagnetic records between the Chinese loess and marine sediments.

Key words: Magnetic fabrics and anisotropy; Palaeointensity; Reversals: process, timescale, magnetostratigraphy; Rock and mineral magnetism.

1 INTRODUCTION

Palaeomagnetic polarity reversals provide useful information not only for studying the dynamic evolution of the Earth's interior, but also for constructing sedimentary age models based on magnetostratigraphy. The Matuyama–Brunhes palaeomagnetic polarity reversal (MBR, ∼780 ka), accompanied by a low field intensity, has been widely recorded in various archives (Love & Mazaud 1997; Clement 2004; Singer *et al.* 2005, and references therein). In addition, an additional decrease in palaeointensity (DIP, Kent & Schneider 1995) of similar magnitude about 20 ka prior to the MBR has also been reported (Hartl & Tauxe 1996; Gratton *et al.* 2007; Brown *et al.* 2009). This was called a 'precursor' to the MBR (MB precursor or MBP hereafter) by Hartl & Tauxe (1996), and has also been observed in marine sediments (Hartl & Tauxe 1996; Guyodo *et al.* 1999; Yamazaki & Oda 2001; Dinares-Turell *et al.* 2002; Carcaillet *et al.* 2003, 2004; Kissel *et al.* 2003; Yamazaki & Oda 2005; Macrì *et al.* 2010; Suganuma *et al.* 2010), lava flows (Quidelleur *et al.* 2002; Singer *et al.* 2002; Brown *et al.* 2004; Petronille *et al.* 2005; Singer *et al.* 2005; Gratton *et al.* 2007), and ice core records (Dreyfus *et al.* 2008). The MBP indicates geomagnetic instability prior to the MBR (Hartl & Tauxe 1996) and can be considered as an independent magnetic feature just preceding the MBR (Kent & Schneider 1995), or as a process by which the magnetic flux diffuses from the solid inner core for sufficiently weakening the geomagnetic stability to allow the reversal to proceed (Singer *et al.* 2005).

Whether the precursor is an individual event or is involved in the MBR process remains uncertain (Raisbeck *et al.* 2006). Magnetic records from volcanic rocks often display discontinuous records of geomagnetic field behaviour (Gratton *et al.* 2007). Marine sediments can preserve continuous recording, but their magnetic signals are easily smoothed or shifted due to lock-in effects (Roberts & Winklhofer 2004). Furthermore, little is known about the MBP recording in terrestrial sediments.

The Chinese loess, as one of the most continuous terrestrial sediments, preserves not only long timescale and high-resolution records of palaeoclimate variability, but also detailed records of geomagnetic field behaviour (Liu *et al.* 2007). However, up to date there is no convincing report of the MBP recorded in Chinese loess. Magnetic anomaly named 'BMPC' (a precursor before the MBR) in the loess unit L9 in the Xi'an and Mangshan sections have been reported by Zheng *et al.* (1992) and (2007), but these anomalies seems to be due to a remagnetization (Wang *et al.* 2005; Jin & Liu 2011a) or to correspond to the Kamikatsura and/or the Santa Rosa geomagnetic excursion events (Yang *et al.* 2004; Wang *et al.* 2010).

Previous studies showed that the recording processes of the natural remanent magnetization (NRM) by loess are complicated (Zhou & Shackleton 1999; Spassov *et al.* 2003; Jin & Liu 2010, 2011a; Spassov *et al.* 2011). To faithfully determine a magnetic polarity reversal boundary or a shortly lived excursion, a statistical approach by using multiple parallel subsamples has been strongly recommended (Jin & Liu 2010). In this study, we will systematically

investigate the palaeomagnetic behaviour from the Luochuan loess section by using such a multiple subsampling scheme. This enables us to test the reliability of the Chinese loess as recorder of the MBP, and provides the basis for discussing its stratigraphic significance.

2 SAMPLING AND EXPERIMENTS

The Luochuan section (35.7°N, 109.4°E) lies in the hinterland of the Chinese Loess Plateau (CLP), northwest of China (Fig. 1), and consists of 33 loess and palaeosol units (~120 m thick) underlain by

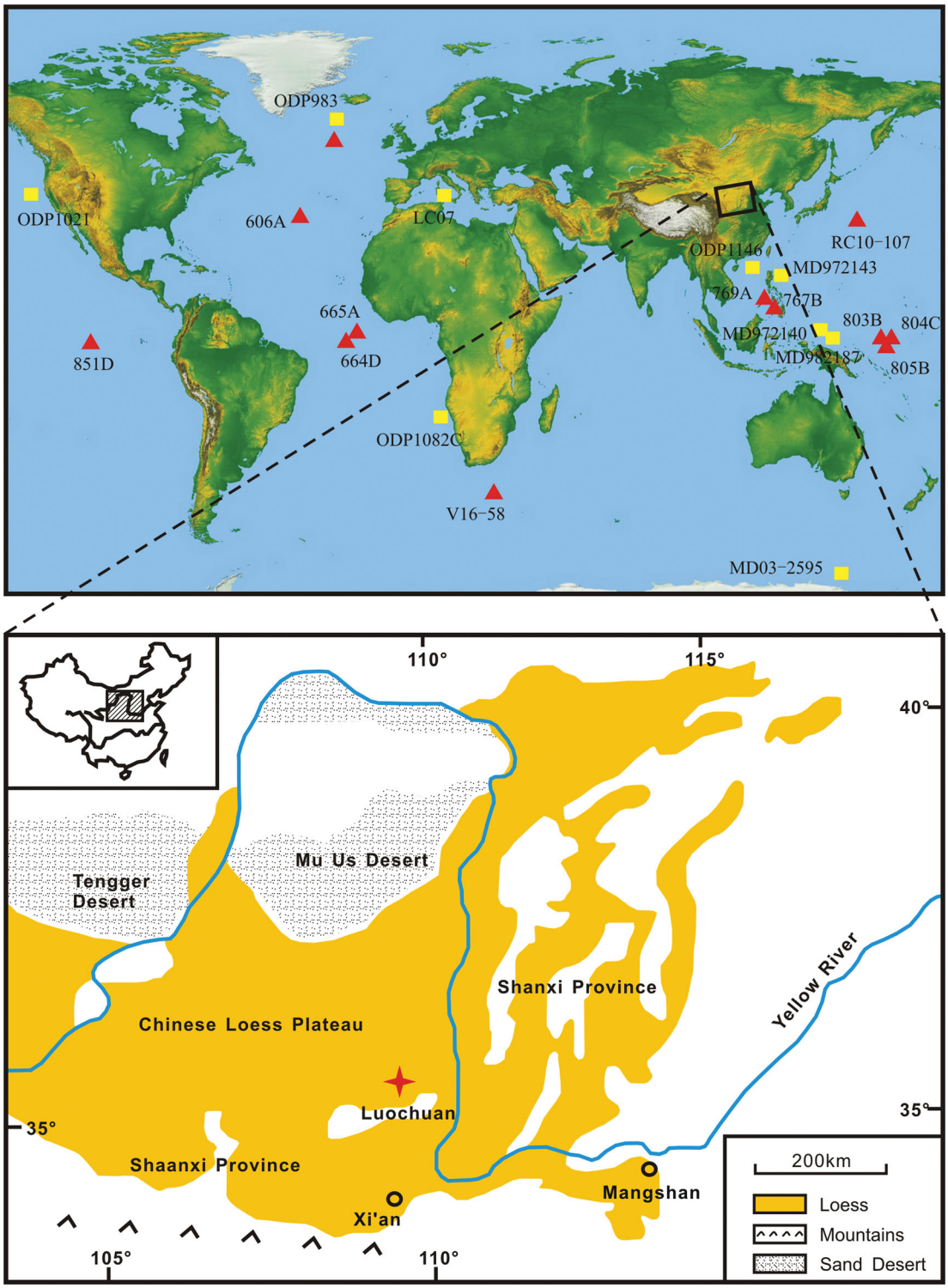

Figure 1. A schematic map showing the Chinese Loess Plateau and distribution of some marine cores recording the Matuyama–Brunhes precursor, such as ODP 1021 (Guyodo *et al.* 1999), ODP 983 (Channell & Kleiven 2000), ODP 1082C (Yamazaki & Oda 2001), LC07 (Dinares-Turell *et al.* 2002), ODP 1146 (Kissel *et al.* 2003), MD 972140 (Carcaillet *et al.* 2003; Carcaillet *et al.* 2004), MD 972143, 982187 (Yamazaki & Oda 2005; Suganuma *et al.* 2010), MD03–2595 (Macrì *et al.* 2010). These cores are shown by squares. The star indicates the Luochuan section. Circles indicate other loess sections mentioned in the text. Triangles indicate the 12 cores compiled by Hartl & Tauxe (1996).

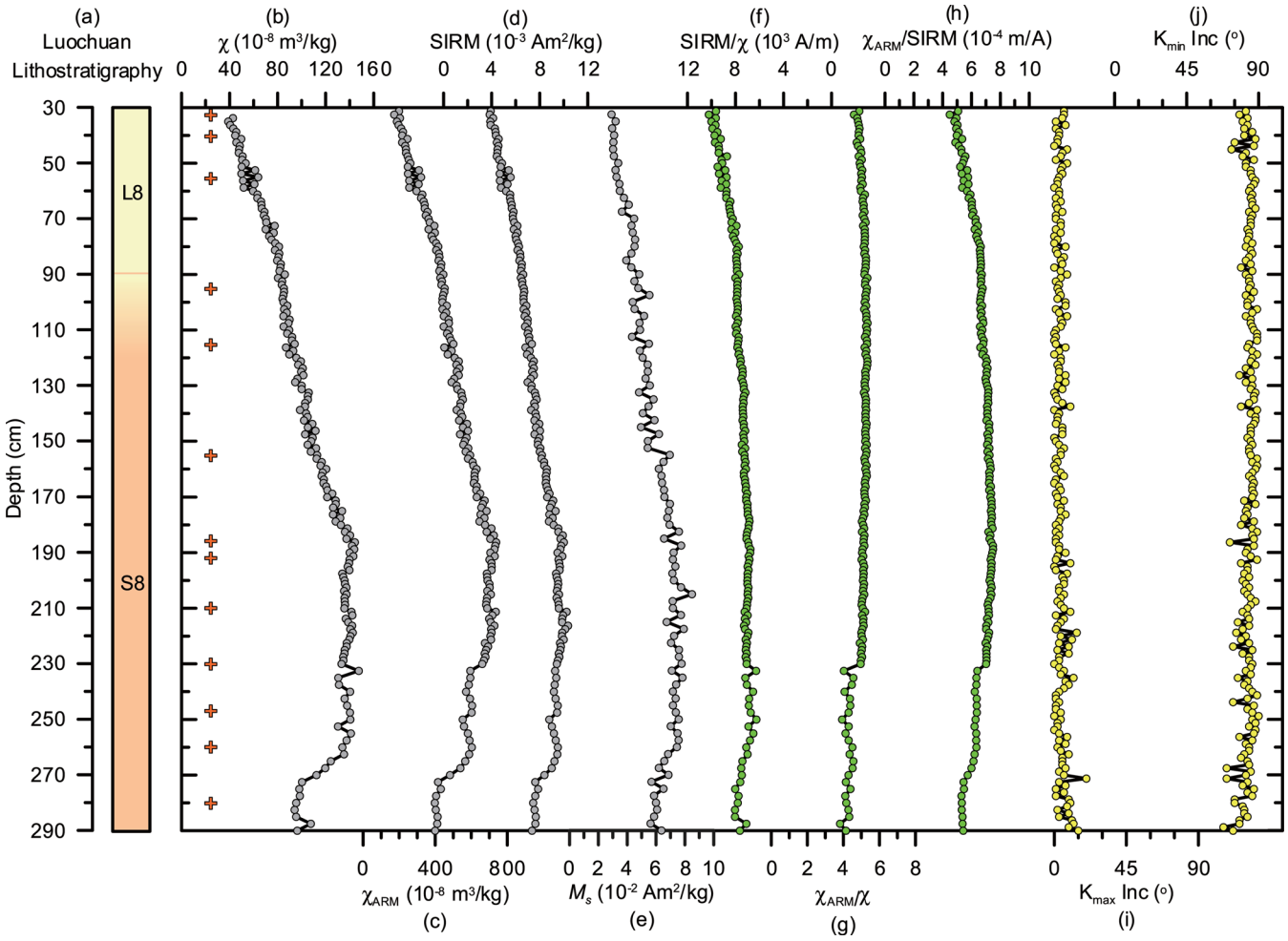

Figure 2. (a) Pedostratigraphy and (b–h) magnetic mineralogical parameters; (i) inclination of maximum-susceptibility axis (K_{max} Inc); (j) inclination of minimum-susceptibility axis (K_{min} Inc).

~10 m thick red clay (Liu 1985). Block samples ($7 \times 7 \times 10$ cm^3) were continuously collected from the loess unit L8 and the palaeosol unit S8 after removing surface weathering cover (pedostratigraphy in Fig. 2a), and were oriented *in situ* using a magnetic compass after sample surface was cut as horizontal as possible. In the lab, the block samples were sawn into 2.5 cm thick slices, and each slice was then cut into six cube specimens ($2 \times 2 \times 2$ cm^3). This resulted in six samples obtained at exactly the same stratigraphic level, with stratigraphic levels sampled at a resolution of ~2.5 cm. Five sets of parallel samples (280 oriented specimens) over 150–290 cm were newly processed for establishing a magnetic stratigraphy. Besides, the sixth set of oriented specimens was used for the normalized parameters for construction of a relative palaeointensity (RPI) record. We define the top of L8 as the zero position.

The low field magnetic susceptibility (χ, mass-specific) of the bulk samples was measured using a Bartington MS2 Susceptibility Meter (Bartington Instruments Ltd., Witney, UK). The anisotropy of magnetic susceptibility (AMS) for all the oriented samples was measured using a KLY-3s Kappabridge (AGICO Ltd., Brno, Czech Republic) before thermal treatment. Bulk samples were selected for detailed rock magnetism analysis (crosses in Fig. 2b). Temperature-dependent susceptibility (χ–T) curves were measured using an MFK1-FA Kappabridge (AGICO Ltd., Brno, Czech Republic) equipped with a CS-4 high-temperature furnace going from room temperature up to 700 °C in an argon atmosphere (the flow rate is about 100 ml min^{-1}) to avoid magnetic mineral alteration upon heating. Temperature-dependent saturation magnetization (M_s–T) curves were measured using a variable field translation balance (VFTB) system (Petersen Instruments, Munich, Germany). Samples for M_s–T curves were heated in air using a field of 1 T. The temperature sweeping rate was 40 °C min^{-1}. Two samples from 35 and 187.5 cm were used for low-temperature (LT) magnetic measurement on a Quantum Designs single-axis superconducting quantum interference device (SQUID) Magnetic Properties Measurement System (MPMS; Quantum Design, San Diego, CA, USA). Prior to LT measurements, the ambient field in the measurement chamber of the MPMS was adjusted to $< \pm 0.5$ μT. Then the two samples were given an LT saturation isothermal remanent magnetization (LT-SIRM), that is, an isothermal remanent magnetization (IRM) acquired in a 2.5 T field at 10 K after zero-field cooling from 300 K. The LT-SIRM demagnetization was measured during warming from 10 to 300 K.

IRM acquisition curves (with a maximum field of 2 T), backfield demagnetization curves and hysteresis parameters [including the saturation magnetization (M_s), saturation remanence (M_{rs}), coercivity (B_c), coercivity of remanence (B_{cr})] were measured using a Princeton Measurements vibrating sample magnetometer (VSM3900; Princeton Measurements Corp., Princeton, NJ, USA). Hysteretic parameters were obtained after subtraction of the paramagnetic contribution. Anhysteretic remanent magnetization (ARM)

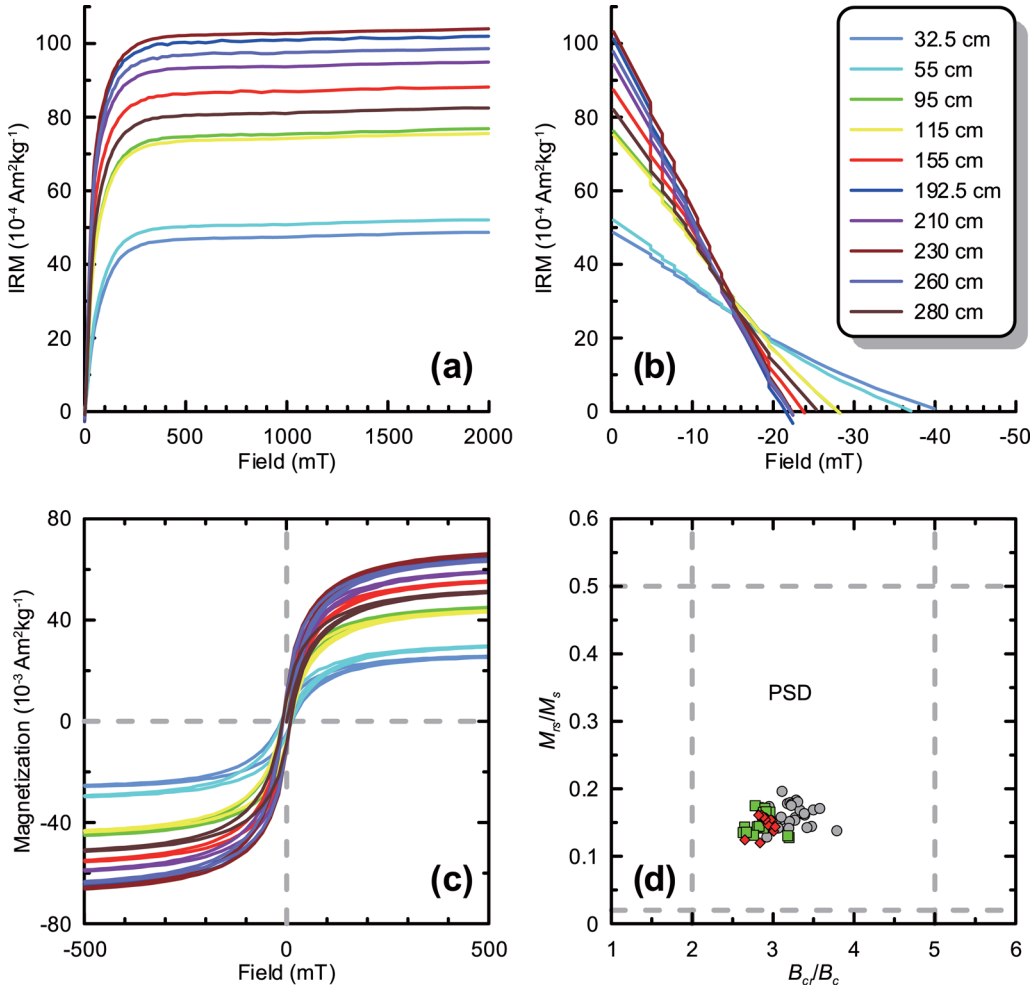

Figure 3. (a) Isothermal remanent magnetization (IRM) acquisition curves. (b) Backfield demagnetization of SIRM. (c) Hysteresis loops, after subtraction of the paramagnetic contribution. (d) Hysteresis ratios plotted on a Day plot (Day *et al.* 1977; Dunlop 2002). Squares and diamonds show samples from the MBR and the MBP, respectively. Circles mean samples from other intervals. PSD, pseudo-single domain. Depth of the measured samples are marked in the legend.

was imparted using an alternating field (AF) with a peak of 100 mT superimposed on a 0.05 mT direct current biased field using a Model 615 anhysteretic remanent magnetizer. The ARM is expressed in terms of the ARM susceptibility (χ_{ARM} = ARM/DC field). SIRM was acquired in a DC field using a 2G660 pulse magnetizer with 1.5 T.

Progressive thermal demagnetization was carried out on all the oriented specimens from room temperature up to 585 or 680 °C using a Magnetic Measurements Thermal Demagnetizer (Magnetic Measurements Ltd., Aughton, UK) with a residual magnetic field of <10 nT. All remanences were measured using a 2G Enterprises Model 760 cryogenic magnetometer (2G Enterprises, Sand City, CA, USA) installed in a magnetically shielded room (<300 nT).

3 RESULTS

3.1 Coercivity analysis

The IRM acquisition curves for representative samples are almost identical. They climb quickly and almost reach saturation at 200 mT (Fig. 3a), which indicates the presence of low-coercivity magnetic minerals such as magnetite and/or maghemite. After 200 mT, the curves increase slightly and do not reach saturation until 2 T, which indicates the presence of high-coercivity magnetic minerals such as haematite and/or goethite. The stepwise demagnetization of SIRM using a DC backfield shows a low B_{cr} (<41 mT) (Fig. 3b).

The hysteresis loops close at about 300 mT (Fig. 3c) and display a weakly wasp-waisted shape representing a mixed assemblage of magnetic minerals with low and high coercivity (Roberts *et al.* 1995). Hysteresis parameter ratios (M_{rs}/M_s, B_{cr}/B_c) were plotted on a Day plot (Day *et al.* 1977; Dunlop 2002) to determine the domain state of magnetic minerals in samples (Fig. 3d). All data cluster tightly within the pseudo-single domain (PSD) field. This indicates that samples throughout the studied sequence are characterized by a magnetic assemblage with a similar grain size and composition.

3.2 Thermomagnetic experiments

Owing to the high sensitivity to the magnetic minerals changes during thermal treatments, the χ–T curve has been widely used as a routine rock magnetic tool to identify magnetic mineralogy and possible mineral transformation upon heating. The M_s–T curve is generally preferred for determining the Curie temperature of natural samples. By combining these two techniques, the complexities due to the thermal alteration on raw samples can be highly reduced. In Figs 4(a) and (b), both the χ–T and M_s–T curves display

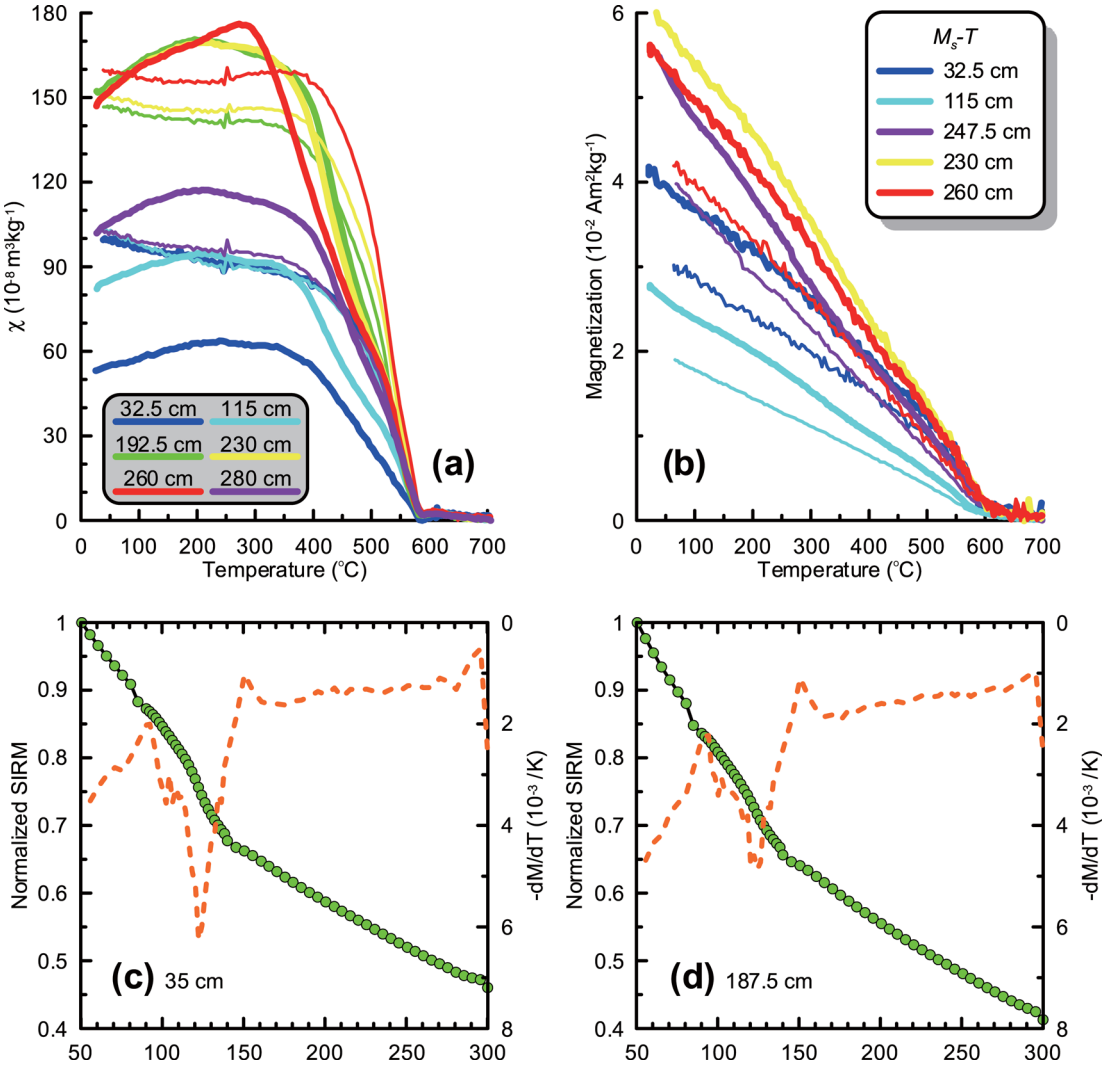

Figure 4. (a) Temperature-dependent susceptibility curves (χ–T curves). (b) Temperature-dependent magnetization (M_s–T curves). Thick (fine) lines indicate heating and cooling, respectively. (c and d) Low-temperature saturation IRM demagnetization curves. Dashed lines are the first derivatives of LT-SIRM curves. Samples for (c) and (d) are from 35 and 187.5 cm, respectively.

distinct decay towards 580 °C for all the selected samples, indicating the Curie temperature of magnetite. In addition, there is a slight concave shape between 300–450 °C of the M_s–T curves during heating. The susceptibility decreases visibly at 300–500 °C for the χ–T curves during heating. The steady magnetic decreases after 300 °C are generally interpreted as the conversion of metastable maghemite to weakly magnetic haematite (Zhu *et al.* 1994a; Liu *et al.* 2005b). For most of the samples, χ–T curves are almost fully reversible for heating and cooling branches, which indicates limited mineral conversion during the thermal treatment. Exceptionally, for the sample from 32.5 cm, the room temperature susceptibility after cooling is twice in magnitude higher than the initial value, which is attributed to the neoformation of magnetite grains from iron-containing silicates/clays or to the formation of magnetite by reduction of haematite due to the burning of organic matter (Deng *et al.* 2004, 2005, 2006; Liu *et al.* 2005b; Deng 2008). However, for the M_s–T curves, the magnetization after cooling is lower than the initial value, indicating that some inversion (e.g. maghemite to haematite) took place during heating (Heller *et al.* 1991; Zhu *et al.* 1994a,b; Liu *et al.* 2003a; Yang *et al.* 2008).

For the LT measurement, both samples display distinct Verwey transitions around 120 K, which is indicative of magnetite (Dunlop & Özdemir 1997) (Figs 4c and d), consistent with previous loess studies (Liu *et al.* 2003b; Deng 2008; Jin & Liu 2011a). These results further support the inferred homogeneity of the magnetic assemblage in both the studied loess (L8) and palaeosoil (S8).

3.3 AMS results

The inclination of maximum-susceptibility axes are <15°, and 98 per cent of the inclinations of minimum-susceptibility axes are >75°, perpendicular to the horizontal plane (Figs 2i and j). The shape of the AMS ellipsoid is oblate and is controlled mainly by foliation (F > 1.003). This indicates that the magnetic fabrics of the studied sediments represent a primary sedimentary fabric without apparent disorder and disturbance (Zhu *et al.* 1999, 2004; Guo *et al.* 2002; Liu *et al.* 2005a; Wang *et al.* 2005; Jin & Liu 2010; Wang *et al.* 2010; Jin & Liu 2011a, b; Fig. 5).

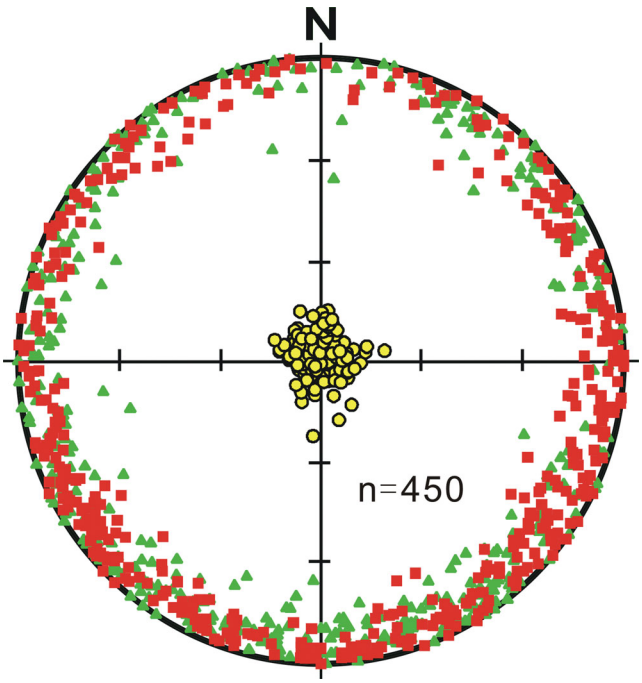

Figure 5. Principal directions of the anisotropy of magnetic susceptibility for the samples in an equal-area stereographic projection. Squares, triangles and circles represent the maximum, intermediate and minimum susceptibility axis, respectively.

3.4 Palaeomagnetic directional results

The NRM contains two magnetic components (Fig. 6). The LT component (<300 °C) of the NRM is commonly considered to be a viscous remanent magnetization (VRM) (e.g. Heller & Liu 1982; Pan *et al.* 2001; Wang *et al.* 2005). The characteristic remanent magnetization (ChRM) for most of the samples (95 per cent) was isolated between 300–500 °C using principal component analysis (Kirschvink 1980; Figs 6b, e, h and k). The magnetic directions are disordered above 580 °C (Figs 6c, f, i and l). This behaviour points to magnetite as the main ChRM carrier. Finally, an abnormal zone of magnetic direction can be clearly determined by five subsets of parallel samples at the interval of 220–270 cm (Fig. 7).

3.5 Relative palaeointensity

Combined palaeo- and rock-magnetic results suggest that PSD detrital magnetite particles of aeolian origin are the dominant remanence carriers in both L8 and S8 in the Luochuan region. Ratios of SIRM/χ, χ_{ARM}/SIRM and χ_{ARM}/χ, which can be used as grain size indicators for magnetite (Evans & Heller 2003), were widely employed in loess studies (e.g. Bloemendal & Liu 2005; Deng *et al.* 2005; Deng 2008; Jin & Liu 2011a). These three ratios vary within a limited range of 6.26×10^3–10.22×10^3 A m^{-1}, 3.82–5.34 and 4.49–7.50 $\times$ 10^{-4} m A^{-1}, respectively (Figs 2f–h), indicating the relative uniform of the magnetic grain size. The magnetic concentrations also change in a limited range (Figs 2b–e). These results indicate that the studied sediments from the Luochuan section satisfy the criteria for establishing reliable RPI records (Tauxe 1993).

The sixth set of samples for RPI normalized parameters was given an ARM first. The ARM was treated with 300 °C thermal demagnetization and then AF of 100 mT demagnetization. Then, SIRM was imparted and followed by another 300 °C thermal demagnetization. The residual magnetization of NRM, ARM and SIRM after 300 °C thermal demagnetization is referred to as NRM300, ARM300 and SIRM300, respectively. Thermal treatments with 300 °C were selected to eliminate influences of the VRM in samples which could be easily removed with thermal demagnetization less than 300 °C. The RPI was represented using NRM300 of each set of parallel specimens which are used for magnetic stratigraphy normalized by χ, ARM300 and SIRM300 to eliminate the contributions of concentration of magnetic grains in samples. All the remanences were mass-specific. The ratios of NRM300/χ, NRM300/ARM300 and NRM300/SIRM300 were normalized by the average of each sequence, respectively (Fig. 8). These ratios have been used by several previous studies, such as NRM300/χ in Zhu *et al.* (1994b), NRM300/ARM300 in Zhu *et al*. (1999) and NRM300/χ, NRM300/ARM300 in Pan *et al*. (2001). The stacked RPI records obtained using the bootstrap method (Tauxe *et al.* 1991) of every ratio for five sets of samples are also similar (Figs 8p–r). There are two clear DIPs at the intervals of 280–200 and 140–50 cm (denoted as DIP1 and DIP2, respectively, Fig. 8), both accompanied with disordered magnetic directions as shown in Fig. 7.

Although curves of NRM300/χ, NRM300/ARM300 and NRM300/SIRM300 resemble each other, SIRM300 was selected to construct the RPI because the SIRM and NRM have similar magnetic carriers in Chinese loess (Liu *et al.* 2005a).

4 DISCUSSION

4.1 Determination of the MBP in Chinese loess

The correlation between the RPI and the corresponding normalizer can be used to test the reliability of the RPI record (Fig. 9). The RPI is linearly related to NRM300 (Figs 9p–t), but not correlated with the corresponding normalizers (Figs 9a–o). This indicates little contamination of the RPI by palaeoclimatic variability. The two DIPs can well be correlated with the ^{10}Be flux peaks (thicker line in Fig. 10a), a proxy inversely correlated to the Earth's magnetic field (Dreyfus *et al.* 2008), and with the two DIPs in the 12 marine cores (Fig. 10c) (Hartl & Tauxe 1996). Such a strong correlation among different records demonstrates that our newly constructed RPI should mainly reflect changes in the geomagnetic palaeointensity.

The uniformity of magnetic minerals and evidence for undisturbed sedimentary fabrics reveal that the magnetic anomaly of both directions and RPI across 270–220 cm and 121–74 cm was not caused by depositional or post-depositional disturbance, or pedogenesis based on the consistence of ChRM directions outside the zones of magnetic anomaly. The disordered magnetic directions were accompanied with clear DIPs in the intervals of 280–200 and 140–50 cm (Fig. 7). These behaviours sufficiently satisfy the criteria summarized by Zhu *et al*. (1999) to determine a geomagnetic event in loess. Therefore, the studied interval indeed recorded two geomagnetic anomaly events. Previous study indicates that DIP2 corresponds to the MBR (Jin & Liu 2010). Then the DIP1 probably coincides with the MBP, which is located in the lower part of S8 (Fig. 10b).

A newly reported high-resolution magnetic stratigraphy of the Luochuan section (Liu *et al.* 2010) provides us an opportunity to estimate the mean accumulation rate (MAR) based on the assumption of a constant accumulation rate for the loess–palaeosol sequences. The MB boundary (MBB) and the upper Jaramillo boundary (UJB) were located at 53 and 67.8 m, respectively (Liu *et al.* 2010). The MAR within the Brunhes chron accounts to 6.79 cm ka^{-1} and that between the UJB and the MBB is about 7.05 cm ka^{-1}, according to

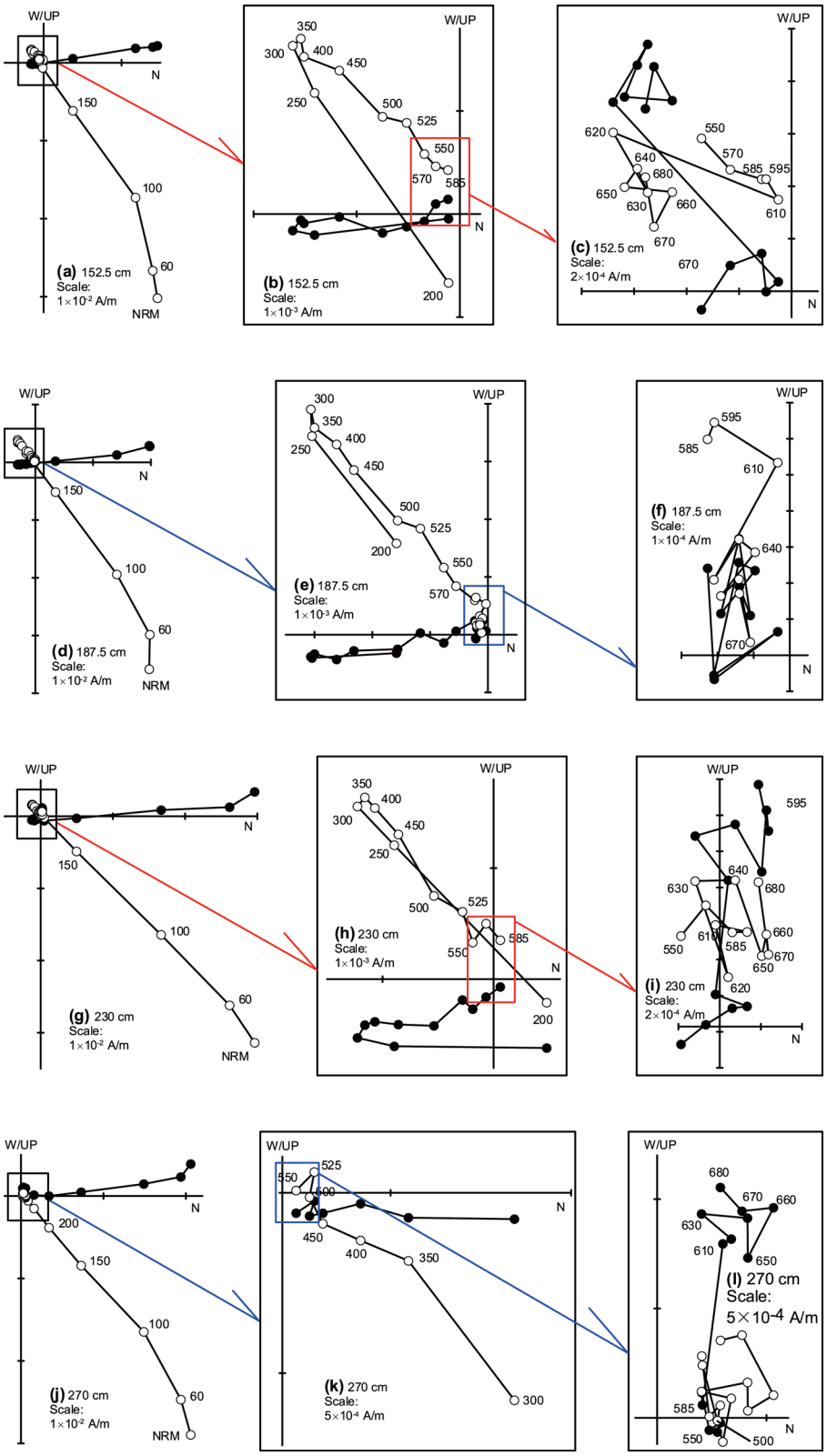

Figure 6. Orthogonal projections of progressive thermal demagnetization of natural remanent magnetization (NRM) for four representative specimens at the Luochuan section at (a–c) 152.5 cm, (d–f) 187.5 cm and (g–i) 230 cm (reverse polarity) and (j–l) 270 cm (normal polarity). Each specimen is shown in three subgraphs marked with different demagnetized temperatures. Solid (open) circles represent projections onto the horizontal (vertical) plane. Demagnetization temperature is given in degrees Celsius.

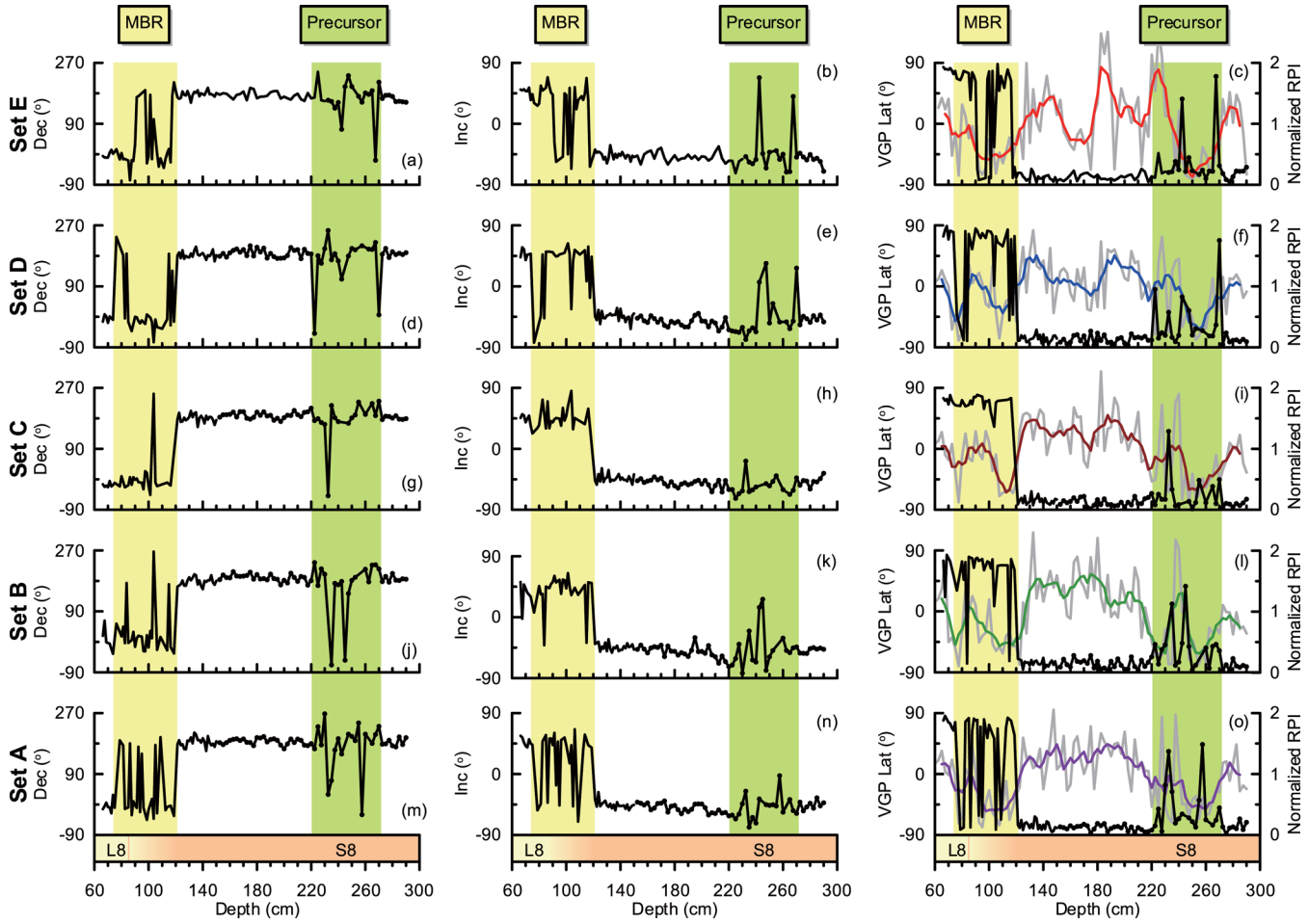

Figure 7. Magnetic stratigraphy (parallel samples Sets A–E) of L8 and S8 in the interval of 60–290 cm at the Luochuan section. Dec, Declination; Inc, Inclination; VGP Lat, virtual geomagnetic pole latitude; MBR, Matuyama–Brunhes reversal. Directional anomalies during the MBR and its precursor are shaded. The colour lines are normalized relative palaeointensity (RPI, refers to NRM300/SIRM300) after five-point smoothing for each subset of parallel samples. Grey lines are background values. NRM300 and SIRM300 are residual magnetization of natural remanent magnetization and saturation isothermal remanent magnetization after 300 °C thermally demagnetization, respectively.

the commonly accepted astrochronological ages for the MBB and the UJB (Shackleton *et al.* 1990). The average of the two MAR is 6.92 cm ka^{-1}. The interval between the midpoints of the two zones of magnetic anomaly is about 147.5 cm thick (Fig. 10b), corresponding to 21.3 ka. This is consistent with records from marine sediments, lava flows and ice cores, where the MBP is always recorded around 20 ka prior to the MBR [e.g. 15–16 ka (Kent & Schneider 1995; Hartl & Tauxe 1996; Yamazaki & Oda 2001; Dinares-Turell *et al.* 2002), 18 ka (Singer *et al.* 2005), 20.5 ka (Channell & Kleiven 2000), 20 ka (Kissel *et al.* 2003), 24 ka (Singer *et al.* 2002) and 23 ka (Dreyfus *et al.* 2008) prior to the MBR; Fig. 10a]. This validates the existence of the MBP in Chinese loess, and gives support for a global nature of the MBP.

Compared to the RPI, the MBP is less well defined by the direction data in this study. Magnetic directions for five sets of parallel samples outside the abnormal intervals (270–220 cm and 121–74 cm) are consistent with each other. For each set of subsample, there are several samples that display first-order excursionary behaviour in the 220–270 cm interval (Fig. 7). However, these behaviours may be counterfeits. The disordered magnetic directions were dominantly caused by the low palaeointensity during anomaly of the geomagnetic field, which could weaken the oriented alignment of the detrital magnetite particles from original source after dust deposition in the CLP (Jin & Liu 2010), further indicating the incapability of loess in the studied area to record rapid geomagnetic reversal information, especially during a low palaeointensity period. Recently, Spassov *et al*. (2011) have simulated the termination recording of the Olduvai subchron in the Lingtai section. They conclude that loess in the central CLP 'are poor candidates for tracking short-term geomagnetic field behaviour such as polarity transitions, geomagnetic excursions and palaeosecular variation', consistent with our previous study (Jin & Liu 2010). Therefore, only the lasting stratigraphic thickness, corresponding to a duration of about 7.2–11.5 ka (estimated by thickness of the direction abnormal zone and the low RPI zone, respectively, based on the accumulation rate of 6.92 cm ka^{-1}), and the stratigraphic location of the MBP, can be defined statistically by using the five sets of direction data. We failed to obtain the detailed geomagnetic field morphology during period of direction anomaly due to the complex processes of NRM recording in Chinese loess (Zhou & Shackleton 1999; Spassov *et al.* 2011). Similar excursionary behaviour during the DIP1 period have also been presented in ODP 805B, 803B, 804C, DSDP 609B cores, which were considered to be affected by either an unremoved or unremovable overprinting (Hartl & Tauxe 1996).

Recent magnetic modelling shows that the course of MB transition is very complex (e.g. Ingham & Turner 2008; Olson *et al.*

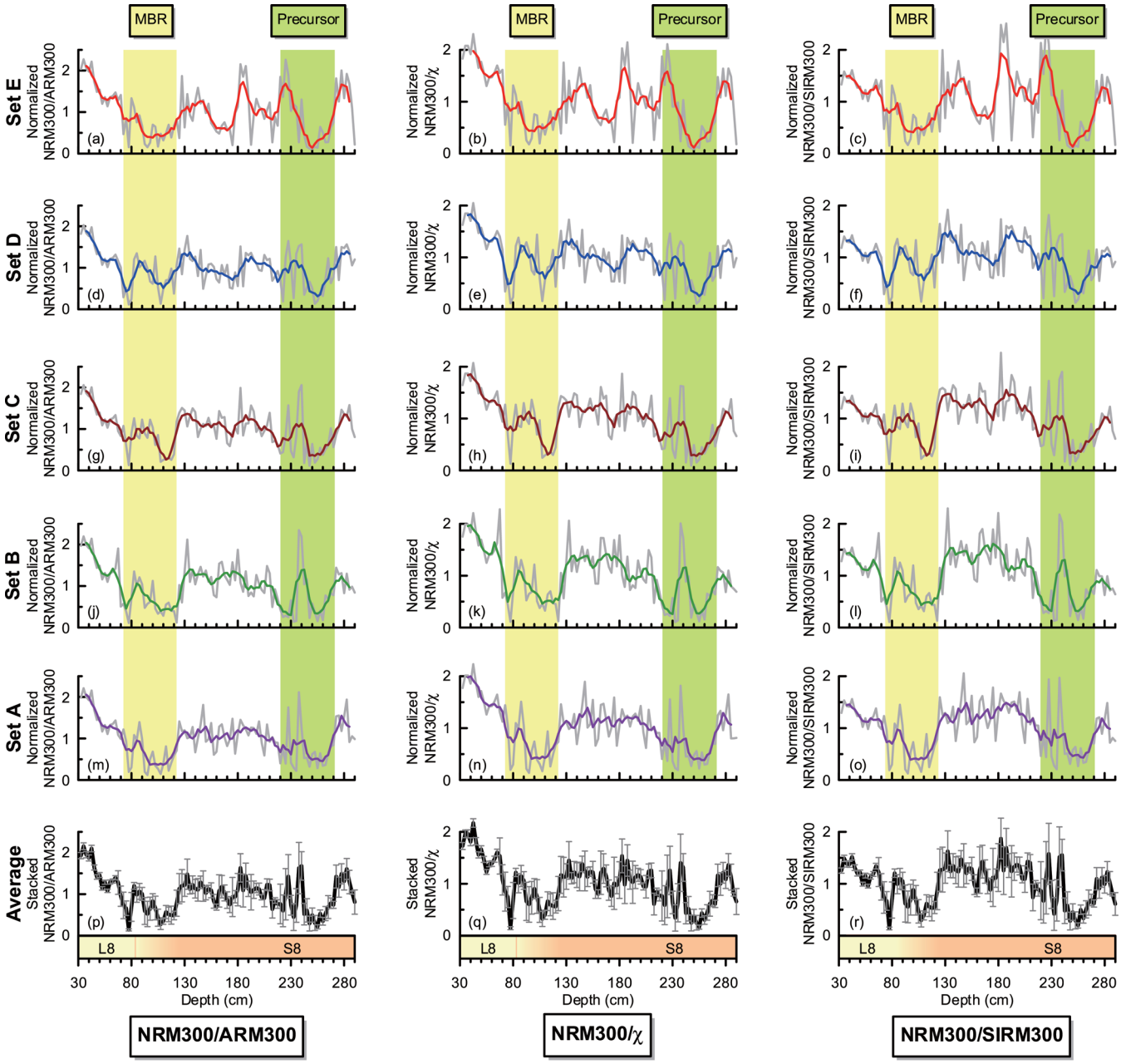

Figure 8. RPI curves constructed from five sets of parallel samples. The colour lines are RPI after five-point smoothing for each subset of parallel samples (a–o). Grey lines are background values. The stack RPI curves are obtained using the bootstrap method (Tauxe *et al.* 1991) of every ratio for five sets of samples (p–r). The error bar responds 95 per cent confidence limits.

2011). About 20 ka prior to the MBR, the dipole field intensity decreased gradually, followed by a precursor period with a multipolar field at the core–mantle boundary. This was followed by the recovery of the dipole and then another decrease that corresponds to the MBR (Olson *et al.* 2011). There is a large patch of reverse flux appearing in the Southern Hemisphere just prior to the MBR (Ingham & Turner 2008). Meanwhile, a similar patch of reverse flux about 15–20 ka prior to the MBR was also observed (Ingham & Turner 2008). Our observations are consistent with these dynamo models. Although the duration and low RPI magnitude of the MBP are comparable to those of the MBR in this study, and are approximately consistent with duration of excursions (5–10 ka) within the Brunhes (Langereis *et al.* 1997), there is no convincing evidence from this study to define the MBP as an individual geomagnetic event. It should therefore be considered as a precursor to the MBR as Kent & Schneider (1995) suggested, marking the transition-field instability from the Matuyama to Brunhes chron (Hartl & Tauxe 1996) and giving therefore support to the dynamo models of Ingham & Turner (2008) and Olson *et al*. (2011).

4.2 Stratigraphic significances

Palaeoclimate records preserved in the Chinese loess can be well correlated with marine sediment records (e.g. Ding *et al.* 2002). However, there is a long-standing debate on the stratigraphic correlation of palaeomagnetic reversal boundaries between marine sediments and loess (Zhu *et al.* 1998; Zhou & Shackleton 1999; Heslop *et al.* 2000; Wang *et al.* 2006; Liu *et al.* 2008). Central to this debate

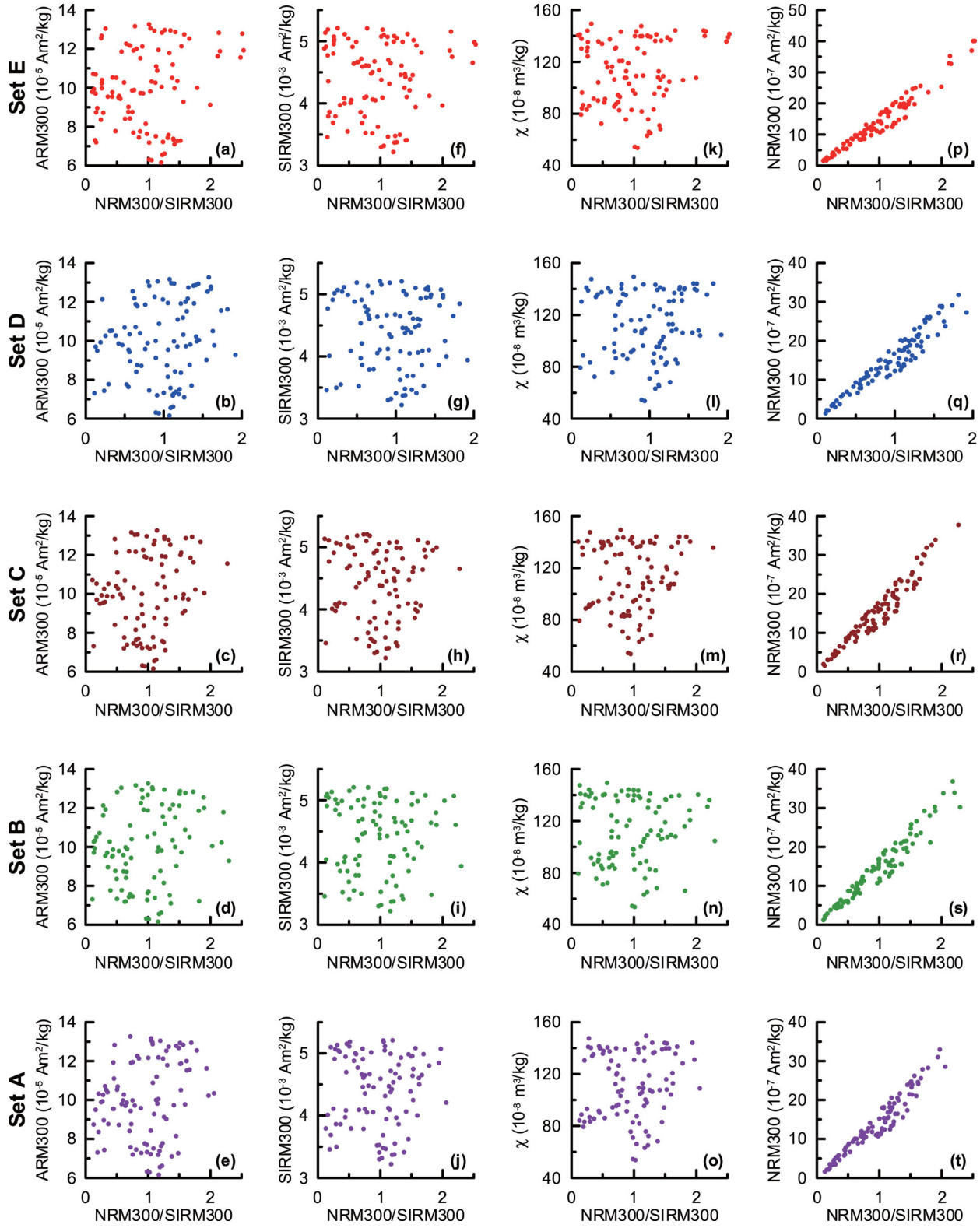

Figure 9. Relativity test between NRM300/SIRM300 with χ, ARM300, SIRM300 and NRM300. NRM300, ARM300 and SIRM300 are residual magnetization of natural remanent magnetization, anhysteretic remanent magnetization and saturation isothermal remanent magnetization after 300 °C thermally demagnetization, respectively.

is the potential NRM lock-in depth in Chinese loess. Large-scale lock-in models proposed that the MBB in Chinese loess has been variably displaced downwards (tens of centimetres to 3 m) from S7 to L8 or S8 in different areas (Zhou & Shackleton 1999). However, this point has been argued by many loess studies in which shallow lock-in depth was proposed (Zhu *et al.* 1994a, 1998, 2006; Pan *et al.* 2002; Wang *et al.* 2006; Liu *et al.* 2008; Yang *et al.* 2008, 2010; Wang & Løvlie 2010). Sedimentological redeposition experiments

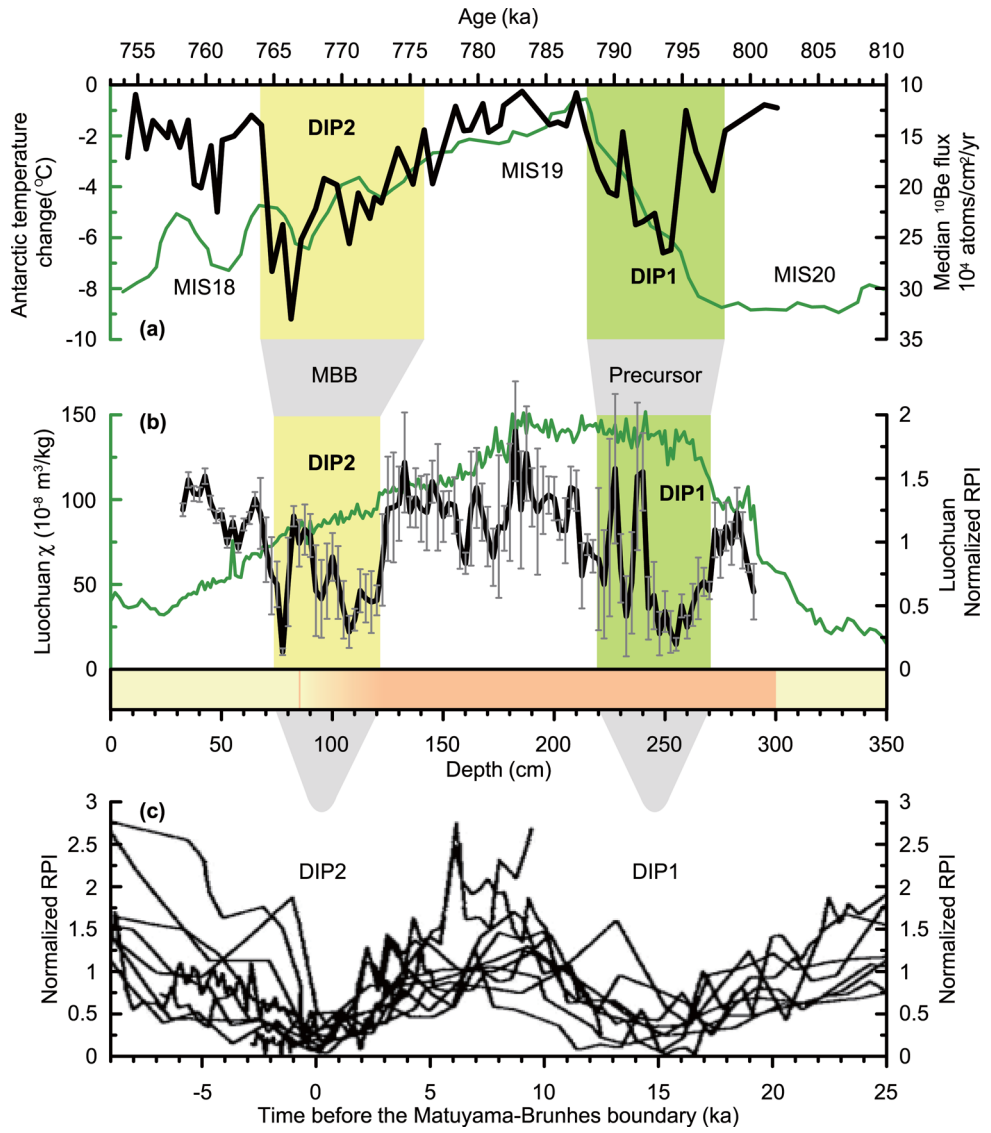

Figure 10. Schematic correlations of stratigraphy and RPI between the Chinese loess, marine sediments and an Antarctic ice core. (a) Thin and thick lines indicate Antarctic temperature change and geomagnetic palaeointensity inferred from the deuterium content (Jouzel *et al.* 2007) and from ^{10}Be flux (the ^{10}Be flux is inversely associated with geomagnetic palaeointensity) of the EPICA Dome C ice core with an improved chronology (Dreyfus *et al.* 2008), respectively. (b) Solid line means a stack RPI (refers to NRM300/SIRM300) calculated using the bootstrap method (Tauxe *et al.* 1991) based on RPI records from five parallel sample sets (colour lines in Fig. 7). The error bar responds 95 per cent confidence limits. Fine line represents magnetic susceptibility. (c) Normalized RPI for 12 marine cores reported by Hartl & Tauxe (1996). DIP1 and DIP2 corresponding to the MBP and MBR are shaded.

suggested that ChRM-carrier magnetic particles in the deposited dusts can be fixed permanently along the ambient field after the initial wetting (Wang & Løvlie 2010) and that the capability of the deposited loess dust to acquire a post-detrital remanent magnetization (pDRM) is enhanced with water content in sediments (Zhao & Roberts 2010). Recently, the termination of the Olduvai subchron recorded in the Lingtai section has been simulated after eliminating the noisy signals during the transition from the upper Olduvai normal polarity to the Matuyama reverse polarity (Spassov *et al.* 2011). Assumption that precursors occurs about 20 ka prior to the transition, the experimental observations are in agreement with the modelled remanence records when the model was calculated with shallower lock-in depths. Meanwhile, the large NRM lock-in depth conflicts with this model (Spassov *et al.* 2011). Indeed, there is a precursor about 21 ka prior to the MBR in the Luochuan area. However, we cannot confirm whether the case model calculation for Lingtai section of Spassov *et al*. (2011) is applicable to the loess in the Luochuan area. It is still difficult to quantify the exact lock-in depth in Chinese loess directly at present. Owing to the complexity of pedogenesis in different areas spatially distributed under different climate condition in the CLP, therefore, caution must be taken to extrapolate the lock-in depth in Chinese loess from this case study. However, it seems spatially consistent for the incapability of loess to record rapid geomagnetic reversal information from case studies in Mangshan (Jin & Liu 2011b), Lingtai (Spassov *et al*. 2011) and Luochuan sections (this study).

A statistical age of 793 ± 3 ka from the ^{40}Ar/^{39}Ar ages of the lavas in Tahiti, Chile and La Palma (Singer *et al.* 2005) is consistent with ages for the MBP from marine sediments, such as 793 ka at ODP 983 (Channell & Kleiven 2000), 788–795 ka at ODP Hole 1082C (Yamazaki & Oda 2001) and 790–795 ka at ODP Holes 767B and 769A (Kent & Schneider 1995) based on oxygen isotope

stratigraphy, associated with 793 ka from the Dome C ice core (Dreyfus *et al.* 2008). These MBP ages were all constrained in the forepart of marine isotope stage (MIS) 19 (Lisiecki & Raymo 2005). Based on the stratigraphic position of the MBP in the lower part of S8 in Chinese loess and in the forepart of MIS 19 in marine sediments, associated with the position of the MBR in the transitional zone between S8 and L8 in loess, and between MIS 19 and 18 in marine sediments, L8 and S8 should be correlated to MIS 18 and 19, respectively (Figs 10a and b).

5 CONCLUSIONS

A high-resolution magnetic stratigraphy for the interval of L8 and S8 reveals two magnetically abnormal zones involving RPI lows and disordered directions in the intervals of 74–121 and 220–270 cm. The former one has been ascribed to the MBR. The latter one is ascribed to a precursor occurred at about 21 ka prior to the MBR, conventionally named MBP. Although detailed morphology cannot be tracked in the studied area, the recording of the MBP in Chinese loess further indicates that the geomagnetic event is probably global in extent and the MB transitional process is complex. The stratigraphic position of the MBR and MBP in Chinese loess and marine sediments further demonstrate the correlation of L8 and S8 to MIS 18 and 19, respectively.

ACKNOWLEDGMENTS

This paper benefited greatly from instructive comments and suggestions by reviewer Yongjae Yu and two other anonymous reviewers, and the editor Andy Biggin. We thank the reviewers for helping to improve the language in a previous version, and Dr Xiang Zhao for helping to calculate the RPI average. This study was supported by the National Natural Science Foundation of China (grants 41004023, 41025013, 40974036, 40821091), the Special Financial Grant from the China Postdoctoral Science Foundation (201104143) and the Science Foundation of the Chinese Academy of Sciences (KZCX2-YW-Q09–02). QL acknowledges further supports from the '100-Talent Program' of the Chinese Academy of Sciences.

REFERENCES

Bloemendal, J. & Liu, X.M., 2005. Rock magnetism and geochemistry of two plio–pleistocene Chinese loess–palaeosol sequences—implications for quantitative palaeoprecipitation reconstruction, *Palaeogeog. Palaeoclimat. Palaeoecol.,* **226,** 149–166.

Brown, L.L., Singer, B.S., Pickens, J.C. & Jicha, B.R., 2004. Paleomagnetic directions and $^{40}Ar/^{39}Ar$ ages from the Tatara-San Pedro volcanic complex, Chilean Andes: Lava record of a Matuyama-Brunhes precursor? *J. geophys. Res.,* **109,** B12101, doi:12110.11029/12004JB003007.

Brown, M.C., Gratton, M.N., Shaw, J., Holme, R. & Soler, V., 2009. Microwave palaeointensity results from the Matuyama-Brunhes geomagnetic field reversal, *Phys. Earth planet. Inter.,* **173,** 75–102.

Carcaillet, J.T., Thouveny, N. & Bourlès, D.L., 2003. Geomagnetic moment instability between 0.6 and 1.3 Ma from cosmonuclide evidence, *Geophys. Res. Lett.,* **30,** 1792, doi:1710.1029/2003GL017550.

Carcaillet, J.T., Bourles, D.L. & Thouveny, N., 2004. Geomagnetic dipole moment and ^{10}Be production rate intercalibration from authigenic $^{10}Be/^{9}Be$ for the last 1.3 Ma, *Geochem. Geophys. Geosyst.,* **5,** Q05006, doi:05010.01029/02003GC000641.

Channell, J.E.T. & Kleiven, H.F., 2000. Geomagnetic palaeointensities and astrochronological ages for the Matuyama-Brunhes boundary and the boundaries of the Jaramillo Subchron: palaeomagnetic and oxygen isotope records from ODP Site 983, *Phil. Trans. R. Soc. Lond., A,* **358,** 1027–1047.

Clement, B.M., 2004. Dependence of the duration of geomagnetic polarity reversals on site latitude, *Nature,* **428,** 637–640.

Day, R., Fuller, M. & Schmidt, V.A., 1977. Hysteresis properties of titanomagnetite: grain-size and compositional dependence, *Phys. Earth planet. Inter.,* **13,** 260–266.

Deng, C.L., 2008. Paleomagnetic and mineral magnetic investigation of the Baicaoyuan loess-paleosol sequence of the western Chinese Loess Plateau over the last glacial-interglacial cycle and its geological implications, *Geochem. Geophys. Geosyst.,* **9,** Q04034, doi:04010.01029/02007GC001928.

Deng, C.L., Zhu, R.X., Verosub, K.L., Singer, M.J. & Vidic, N.J., 2004. Mineral magnetic properties of loess/paleosol couplets of the central loess plateau of China over the last 1.2 Myr, *J. geophys. Res.,* **109,** B01103, doi:01110.01029/02003JB002532.

Deng, C.L., Vidic, N.J., Verosub, K.L., Singer, M.J., Liu, Q.S., Shaw, J. & Zhu, R.X., 2005. Mineral magnetic variation of the Jiaodao Chinese loess//paleosol sequence and its bearing on long-term climatic variability, *J. geophys. Res.,* **110,** B03103, doi:03110.01029/02004JB003451.

Deng, C.L., Shaw, J., Liu, Q.S., Pan, Y.X. & Zhu, R.X., 2006. Mineral magnetic variation of the Jingbian loess/paleosol sequence in the northern Loess Plateau of China: implications for Quaternary development of Asian aridification and cooling, *Earth planet. Sci. Lett.,* **241,** 248–259.

Dinares-Turell, J., Sagnotti, L. & Roberts, A.P., 2002. Relative geomagnetic paleointensity from the Jaramillo Subchron to the Matuyama/Brunhes boundary as recorded in a Mediterranean piston core, *Earth planet. Sci. Lett.,* **194,** 327–341.

Ding, Z.L., Derbyshire, E., Yang, S.L., Yu, Z.W. & Xiong, S.F., 2002. Stacked 2.6-Ma grain size record from the Chinese loess based on five sections and correlation with the deep-sea $\delta^{18}O$ record, *Paleoceanography,* **17,** 1033, doi:1010.1029/2001PA000725.

Dreyfus, G.B., Raisbeck, G.M., Parrenin, F., Jouzel, J., Guyodo, Y., Nomade, S. & Mazaud, A., 2008. An ice core perspective on the age of the Matuyama-Brunhes boundary, *Earth planet. Sci. Lett.,* **274,** 151–156.

Dunlop, D.J., 2002. Theory and application of the Day plot (M_{rs}/M_s versus H_{cr}/H_c) 2. Theoretical curves and tests using titanomagnetite data, *J. geophys. Res.,* **107,** 2057, doi:2010.1029/2001JB000487.

Dunlop, D.J. & Özdemir, Ö., 1997. *Rock Magnetism: Fundamentals and Frontiers,* Cambridge University Press, New York, NY.

Evans, M.E. & Heller, F., 2003. *Environmental Magnetism: Principles and Applications of Enviromagnetics,* Academic Press, New York, NY.

Gratton, M.N., Shaw, J. & Brown, L.L., 2007. Absolute palaeointensity variation during a precursor to the Matuyama-Brunhes transition recorded in Chilean lavas, *Phys. Earth planet. Inter.,* **162,** 61–72.

Guo, B., Zhu, R.X., Florindo, F., Ding, Z.L. & Sun, J.M., 2002. A short, reverse polarity interval within the Jaramillo subchron: evidence from the Jingbian section, northern Chinese Loess Plateau, *J. geophys. Res.,* **107,** doi:10.1029/2001JB000706.

Guyodo, Y., Richter, C. & Valet, J.P., 1999. Paleointensity record from Pleistocene sediments (1.4–0 Ma) off the California Margin, *J. geophys. Res.,* **104,** 22 953–22 964.

Hartl, P. & Tauxe, L., 1996. A precursor to the Matuyama/Brunhes transition-field instability as recorded in pelagic sediments, *Earth planet. Sci. Lett.,* **138,** 121–135.

Heller, F. & Liu, T.S., 1982. Magnetostratigraphical dating of loess deposits in China, *Nature,* **300,** 431–433.

Heller, F., Liu, X.M., Liu, T.S. & Xu, T.C., 1991. Magnetic susceptibility of loess in China, *Earth planet. Sci. Lett.,* **103,** 301–310.

Heslop, D., Langereis, C.G. & Dekkers, M.J., 2000. A new astronomical timescale for the loess deposits of Northern China, *Earth planet. Sci. Lett.,* **184,** 125–139.

Ingham, M. & Turner, G., 2008. Behaviour of the geomagnetic field during the Matuyama-Brunhes polarity transition, *Phys. Earth planet. Inter.,* **168,** 163–178.

Jin, C.S. & Liu, Q.S., 2010. Reliability of the natural remanent magnetization recorded in Chinese loess, *J. geophys. Res.,* **115,** B04103, doi:04110.01029/02009JB006703.

Jin, C.S. & Liu, Q.S., 2011a. Remagnetization mechanism and a new age model for L9 in Chinese loess, *Phys. Earth planet. Inter.,* **187,** 261–275.

Jin, C.S. & Liu, Q.S., 2011b. Revisiting the stratigraphic position of the Matuyama-Brunhes geomagnetic polarity boundary in Chinese loess, *Palaeogeog. Palaeoclimat. Palaeoecol.,* **299,** 309–317.

Jouzel, J. *et al*., 2007. Orbital and millennial Antarctic climate variability over the past 800,000 years, *Science,* **317,** 793–796.

Kent, D.V. & Schneider, D.A., 1995. Correlation of paleointensity variation records in the Brunhes/Matuyama polarity transition interval, *Earth planet. Sci. Lett.,* **129,** 135–144.

Kirschvink, J.L., 1980. The least-squares line and plane and the analysis of palaeomagnetic data, *Geophys. J. R. astr. Soc.,* **62,** 699–718.

Kissel, C., Laj, C., Clemens, S. & Solheid, P., 2003. Magnetic signature of environmental changes in the last 1.2 Myr at ODP Site 1146, South China Sea, *Mar. Geol.,* **201,** 119–132.

Langereis, C.G., Dekkers, M.J., deLange, G.J., Paterne, M. & vanSantvoort, P.J.M., 1997. Magnetostratigraphy and astronomical calibration of the last 1.1 Myr from an eastern Mediterranean piston core and dating of short events in the Brunhes, *Geophys. J. Int.,* **129,** 75–94.

Lisiecki, L.E. & Raymo, M.E., 2005. A Pliocene-Pleistocene stack of 57 globally distributed benthic δ^{18}O records, *Paleoceanography,* **20,** PA1003, doi:1010.1029/2004PA001071.

Liu, Q.S., Banerjee, S.K. & Jackson, M.J., 2003a. An integrated study of the grain-size-dependent magnetic mineralogy of the Chinese loess/paleosol and its environmental significance, *J. geophys. Res.,* **108,** 2437, doi:2410.1029/2002JB002264.

Liu, Q.S., Jackson, M.J., Banerjee, S.K., Zhu, R.X., Pan, Y.X. & Chen, F.H., 2003b. Determination of magnetic carriers of the characteristic remanent magnetization of Chinese loess by low-temperature demagnetization, *Earth planet. Sci. Lett.,* **216,** 175–186.

Liu, Q.S., Banerjee, S.K., Jackson, M.J., Deng, C.L., Pan, Y.X. & Zhu, R.X., 2005a. Inter-profile correlation of the Chinese loess/paleosol sequences during Marine Oxygen Isotope Stage 5 and indications of pedogenesis, *Quat. Sci. Rev.,* **24,** 195–210.

Liu, Q.S., Deng, C.L., Yu, Y., Yorrent, J., Jackson, M.J., Banerjee, S.K. & Zhu, R.X., 2005b. Temperature dependence of magnetic susceptibility in an argon environment: implications for pedogenesis of Chinese loess/palaeosols, *Geophys. J. Int.,* **161,** 102–112.

Liu, Q.S., Deng, C.L., Torrent, J. & Zhu, R.X., 2007. Review of recent developments in mineral magnetism of the Chinese loess, *Quat. Sci. Rev.,* **26,** 368–385.

Liu, Q.S., Roberts, A.P., Rohling, E.J., Zhu, R.X. & Sun, Y.B., 2008. Post-depositional remanent magnetization lock-in and the location of the Matuyama–Brunhes geomagnetic reversal boundary in marine and Chinese loess sequences, *Earth planet. Sci. Lett.,* **275,** 102–110.

Liu, T.S., 1985. *Loess and the Environment,* China Ocean Press, Beijing.

Liu, W.M., Zhang, L.Y. & Sun, J.M., 2010. High resolution magnetostratigraphy of the Luochuan loess-paleosol sequence in the central Chinese Loess Plateau, *Chin. J. Geophys.,* **53,** 888–894 (in Chinese with English abstract).

Love, J.J. & Mazaud, A., 1997. A database for the Matuyama-Brunhes magnetic reversal, *Phys. Earth planet. Inter.,* **103,** 207–245.

Macrì, P., Sagnotti, L., Dinarès-Turell, J. & Caburlotto, A., 2010. Relative geomagnetic paleointensity of the Brunhes Chron and the Matuyama–Brunhes precursor as recorded in sediment core from Wilkes Land Basin (Antarctica), *Phys. Earth planet. Inter.,* **179,** 72–86.

Olson, P.L., Glatzmaier, G.A. & Coe, R.S., 2011. Complex polarity reversals in a geodynamo model, *Earth planet. Sci. Lett.,* **304,** 168–179.

Pan, Y.X., Zhu, R.X., Shaw, J., Liu, Q.S. & Guo, B., 2001. Can relative paleointensities be determined from the normalized magnetization of the wind-blown loess of China?, *J. geophys. Res.,* **106,** 19 221–19 232.

Pan, Y.X., Zhu, R.X., Liu, Q.S., Guo, B., Yue, L.P. & Wu, H.N., 2002. Geomagnetic episodes of the last 1.2 Myr recorded in Chinese loess, *Geophys. Res. Lett.,* **29**(8), 1282, doi:10.1029/2001GL014024.

Petronille, M., Goguitchaichvili, A., Henry, B., Alva-Valdivia, L.M., Rosas-Elguera, J., Urrutia-Fucugauchi, J., Ceja, M.R. & Calvo-Rathert, M., 2005. Paleomagnetism of Ar-Ar dated lava flows from the Ceboruco-San Pedro volcanic field (western Mexico): evidence for the Matuyama-Brunhes transition precursor and a fully reversed geomagnetic event in the Brunhes chron, *J. geophys. Res.,* **110,** B08101, doi:08110.01029/02004JB003321.

Quidelleur, X., Carlut, J., Gillot, P.-Y. & Soler, V., 2002. Evolution of the geomagnetic field prior to the Matuyama-Brunhes transition: radiometric dating of a 820 ka excursion at La Palma, *Geophys. J. Int.,* **151,** F6–F10.

Raisbeck, G.M., Yiou, F., Cattani, O. & Jouzel, J., 2006. ^{10}Be evidence for the Matuyama-Brunhes geomagnetic reversal in the EPICA Dome C ice core, *Nature,* **444,** 82–84.

Roberts, A.P. & Winklhofer, M., 2004. Why are geomagnetic excursions not always recorded in sediments? Constraints from post-depositional remanent magnetization lock-in modelling, *Earth planet. Sci. Lett.,* **227,** 345–359.

Roberts, A.P., Cui, Y.L. & Verosub, K.L., 1995. Wasp-waisted hysteresis loops: mineral magnetic characteristics and discrimination of components in mixed magnetic systems, *J. geophys. Res.,* **100,** 17 909–17 924.

Shackleton, N.J., Berger, A. & Peltier, W.R., 1990. An alternative astronomical calibration of the lower Pleistocene timescale based on ODP Site 677, *Trans. R. Soc. Edinburgh: Earth Sci.,* **81,** 251–261.

Singer, B.S., Relle, M.K., Hoffman, K.A., Battle, A., Laj, C., Guillou, H. & Carracedo, J.C., 2002. Ar/Ar ages from transitionally magnetized lavas on La Palma, Canary Islands, and the geomagnetic instability timescale, *J. geophys. Res.,* **107**(B11), 2307, doi:2310.1029/2001JB001613.

Singer, B.S., Hoffman, K.A., Coe, R.S., Brown, L.L., Jicha, B.R., Pringle, M.S. & Chauvin, A., 2005. Structural and temporal requirements for geomagnetic field reversal deduced from lava flows, *Nature,* **434,** 633–636.

Spassov, S., Heller, F., Evans, M.E., Yue, L.P. & von Dobeneck, T., 2003. A lock-in model for the complex Matuyama-Brunhes boundary record of the loess/palaeosol sequence at Lingtai (Central Chinese Loess Plateau), *Geophys. J. Int.,* **155,** 350–366.

Spassov, S., Hus, J., Heller, F., Evans, M.E., Yue, L.P. & von Dobeneck, T., 2011. The termination of the Olduvai Subchron at Lingtai, Chinese Loess Plateau: geomagnetic field behavior or complex remanence acquisition? in *The Earth's Magnetic Interior, IAGA Special Sopron Book Series 1,* pp. 235–245, eds Petrovský, E., Ivers, D., Harinarayana, T. & Herrero-Bervera, E., Springer, New York, NY.

Suganuma, Y., Yokoyama, Y., Yamazaki, T., Kawamura, K., Horng, C.-S. & Matsuzaki, H., 2010. ^{10}Be evidence for delayed acquisition of remanent magnetization in marine sediments: implication for a new age for the Matuyama-Brunhes boundary, *Earth planet. Sci. Lett.,* **296,** 443–450.

Tauxe, L., 1993. Sedimentary records of relative paleointensity of the geomagnetic field: theory and practice, *Rev. Geophys.,* **31,** 319–354.

Tauxe, L., Kylstra, N. & Constable, C., 1991. Bootstrap statistics for paleomagnetic data, *J. geophys. Res.,* **96,** 11 723–11 740.

Wang, R.H. & Løvlie, R., 2010. Subaerial and subaqueous deposition of loess: experimental assessment of detrital remanent magnetization in Chinese loess, *Earth planet. Sci. Lett.,* **298,** 394–404, doi:10.1016/j.epsl.2010.1008.1019.

Wang, X.S., Løvlie, R., Yang, Z.Y., Pei, J.L., Zhao, Z.Z. & Sun, Z.M., 2005. Remagnetization of Quaternary eolian deposits: a case study from SE Chinese Loess Plateau, *Geochem. Geophys. Geosyst.,* **6,** Q06H18, doi:10.1029/2004GC000901.

Wang, X.S., Yang, Z.Y., Løvlie, R., Sun, Z.M. & Pei, J.L., 2006. A magnetostratigraphic reassessment of correlation between Chinese loess and marine oxygen isotope records over the last 1.1 Ma, *Phys. Earth planet. Inter.,* **159,** 109–117.

Wang, D.J., Wang, Y.C., Han, J.T., Duan, M.G., Shan, J.Z. & Liu, T.S., 2010. Geomagnetic anomalies recorded in L9 of the Songjiadian loess section in southeastern Chinese Loess Plateau, *Chin. Sci. Bull.,* **55,** 520–529.

Yamazaki, T. & Oda, H., 2001. A Brunhes-Matuyama polarity transition record from anoxic sediments in the South Atlantic (Ocean Drilling Program Hole 1082C), *Earth Planets Space,* **53,** 817–827.

Yamazaki, T. & Oda, H., 2005. A geomagnetic paleointensity stack between 0.8 and 3.0 Ma from equatorial Pacific sediment cores, *Geochem. Geophys. Geosyst.,* **6,** doi:10.1029/2005GC001001.

Yang, T.S., Hyodo, M., Yang, Z.Y. & Fu, J.L., 2004. Evidence for the Kamikatsura and Santa Rosa excursions recorded in eolian deposits

from the southern Chinese Loess Plateau, *J. geophys. Res.,* **109,** B12105, doi:12110.11029/12004JB002966.

Yang, T.S. *et al*., 2008. Latest Olduvai short-lived reversal episodes recorded in Chinese loess, *J. geophys. Res.,* **113,** B05103, doi:05110.01029/02007JB005264.

Yang, T.S., Hyodo, M., Yang, Z.Y., Li, H.D. & Maeda, M., 2010. Multiple rapid polarity swings during the Matuyama-Brunhes (M-B) transition from two high-resolution loess-paleosol records, *J. geophys. Res.,* **115,** B05101, doi:05110.01029/02009JB006301.

Zhao, X. & Roberts, A.P., 2010. How does Chinese loess become magnetized? *Earth planet. Sci. Lett.,* **292,** 112–122.

Zheng, H.B., An, Z.S. & Shaw, J., 1992. New contributions to Chinese Plio-Pleistocene magnetostratigraphy, *Phys. Earth planet. Inter.,* **70,** 146–153.

Zheng, H.B., Huang, X.T., Ji, J.L., Liu, R., Zeng, Q.Y. & Jiang, F.C., 2007. Ultra-high rates of loess sedimentation at Zhengzhou since State 7: implication for the Yellow River erosion of the Sanmen Gorge, *Geomorphology,* **85,** 131–142.

Zhou, L.P. & Shackleton, N.J., 1999. Misleading positions of geomagnetic reversal boundaries in Eurasian loess and implications for correlation between continental and marine sedimentary sequences, *Earth planet. Sci. Lett.,* **168,** 117–130.

Zhu, R.X., Laj, C. & Mazaud, A., 1994a. The Matuyama-Brunhes and Upper Jaramillo transitions recorded in a loess section at Weinan, north-central China, *Earth planet. Sci. Lett.,* **125,** 143–158.

Zhu, R.X., Zhou, L.P., Laj, C., Mazaud, A. & Ding, Z.L., 1994b. The Blake geomagnetic polarity episode recorded in Chinese loess, *Geophys. Res. Lett.,* **21,** 697–700.

Zhu, R.X., Pan, Y.X., Guo, B. & Liu, Q.S., 1998. A recording phase lag between ocean and continent climate changes: constrained by the Matuyama/Brunhes polarity boundary, *Chin. Sci. Bull.,* **43,** 1593–1598.

Zhu, R.X., Pan, Y.X. & Liu, Q.S., 1999. Geomagnetic excursions recorded in Chinese loess in the last 70,000 years, *Geophys. Res. Lett.,* **26,** 505–508.

Zhu, R.X., Liu, Q.S. & Jackson, M.J., 2004. Paleoenvironmental significance of the magnetic fabrics in Chinese loess-paleosols since the last interglacial (<130 ka), *Earth planet. Sci. Lett.,* **221,** 55–69.

Zhu, R.X., Liu, Q.S., Pan, Y.X., Deng, C.L., Zhang, R. & Wang, X.F., 2006. No apparent lock-in depth of the Laschamp geomagnetic excursion: evidence from the Malan loess, *Sci. China, D, Earth Sci.,* **49,** 960–967.